J. Phys. B: At. Mol. Opt. Phys. **32** (1999) 1001–1008. Printed in the UK PII: S0953-4075(99)97893-8

Time-dependent kinetics model for a helium discharge plasma

J Abdallah Jr†‡, N Palmer†, W Gekelman†, J Maggs† and R E H Clark‡

† Department of Physics University of California, Los Angeles, CA 90095, USA
‡ Los Alamos National Laboratory Los Alamos, NM 87545, USA

Received 29 September 1998, in final form 7 December 1998

Abstract. Measurements of electron density and electron temperature at various times during a cathode discharge in helium have been recorded with a Langmuir probe in the UCLA large plasma device. The measured electron temperatures were then used in a time-dependent collisional–radiative model to propagate the electron density as a function of time for plasma conditions corresponding to population densities far from equilibrium. The initial gas density was extracted from pressure measurements and used in the calculations so there were no adjustable parameters in the model. The calculated and measured densities are in good agreement for three different radial positions in the plasma. The results show that the plasma formation becomes dominated by bulk thermal electrons early in the discharge. The detailed model is compared with several simplified models to study the role of metastable levels and excited states in the plasma kinetics. The relative importance of the various atomic processes in the calculation of plasma formation is also discussed.

1. Introduction

The large plasma device (LAPD) at UCLA is a linear plasma research facility (Gekelman *et al* 1991, Pfister *et al* 1991) primarily designed to study space plasma processes. A 10 m long plasma column with a diameter of 40 cm is created with densities in the 10^{12}–10^{13} cm^{-3} range and electron temperatures in the 5–10 eV range. The geometry is well suited for making localized measurements of the plasma conditions. Helium and argon gases are generally used in the discharge. At early times in the discharge, the electron density builds up quickly due to the interaction of energetic primary electrons with the target gas producing secondary electrons from collisional ionization. In this phase, the electron energy distribution is highly non-Maxwellian, and the ionization rate of the plasma is unusually rapid. This phase will be the subject of future study. The bulk of the density is quickly formed by secondary electrons which are Maxwellian in nature. The subsequent ionization is then dominated by these thermal electrons. Ionization in the plasma continues until the discharge current is switched off. The purpose of this paper is to study the kinetics of plasma formation in the LAPD during this long-lived phase in which ionization and excitation are dominated by bulk thermal electrons.

The electron density and electron temperature have been measured in the LAPD plasma at various times and locations during the discharge. These measurements have been compared with the results of detailed atomic kinetics calculations using the Los Alamos suite of atomic physics codes (Abdallah *et al* 1996). Time dependency is required because the lifetime of the LAPD plasma is short (milliseconds) compared with the steady-state equilibration times (tenths of seconds). Hence, the LAPD plasma is underionized compared to steady-state predictions at the temperatures that are typically encountered. Previous collisional radiative calculations for helium (Fujimoto 1979, Goto and Fujimoto 1997) have considered only steady-state properties.

0953-4075/99/041001+08$19.50

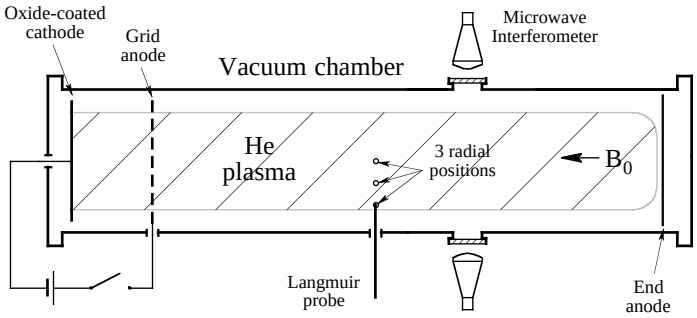

Figure 1. Schematic diagram of the LAPD.

In this paper, the coupled rate equations are solved as a function of time to predict level populations and free electron density. The predicted electron densities are compared with the measured values. The calculation, which involves no adjustable parameters, provides insight into plasma formation in the LAPD as well as a validation of the atomic physics model. Plans for future study include a comparison of calculated spectral line intensities with optical measurements to validate the populations of individual energy levels.

2. Experiment

A schematic diagram of the LAPD is shown in figure 1. For this experiment, the 40 cm diameter oxide-coated cathode produced a 2.95 kA discharge current with a discharge voltage near 50 V. The duration of the discharge pulse was about 3 ms, and the repetition rate was 1 Hz. The chamber was filled with helium at a pressure of 1.1×10^{-4} torr which corresponds to a gas density of 2.6×10^{12} cm^{-3}. For confinement, a uniform axial magnetic field (B_0) of 1200 G was generated by solenoidal magnet coils around the machine.

The electron density and temperature were measured at various times during the discharge using a Langmuir probe and microwave interferometry. The probe measurements alone do not yield absolute values for plasma density because the background magnetic field constrains the magnitude of the current collected by the probe. To compensate, we use the microwave interferometer to measure the line-integrated phase shift across the diameter of the plasma, which is directly related to the line integral of the plasma density profile. We then take 50–60 Langmuir probe measurements across the diameter of the plasma, which yields a radial plasma density profile of relative magnitude. By numerically integrating the measured density profile and scaling it to produce a computed phase shift equal to the measured phase shift, we effectively calibrate our Langmuir probe density measurments for a given magnetic field and range of plasma parameters.

In contrast, our Langmuir probe temperature measurements are largely independent of magnetic field because they do not rely on the absolute magnitude of the probe current. Rather, they are based on the measured rate at which the current transitions from ion to electron saturation in response to the change in the applied voltage. Since the charges are free to move along the magnetic field, this rate is predominantly determined by the axial electron distribution function, and the probe signal accurately reflects that distribution. Langmuir probe measurements of electron temperature have been corroborated by whistler and Alfvén wave propagation studies done on this device (Bamber *et al* 1995, Gekelman *et al* 1997).

The electron density and temperature measurements for this study are presented in figure 2.

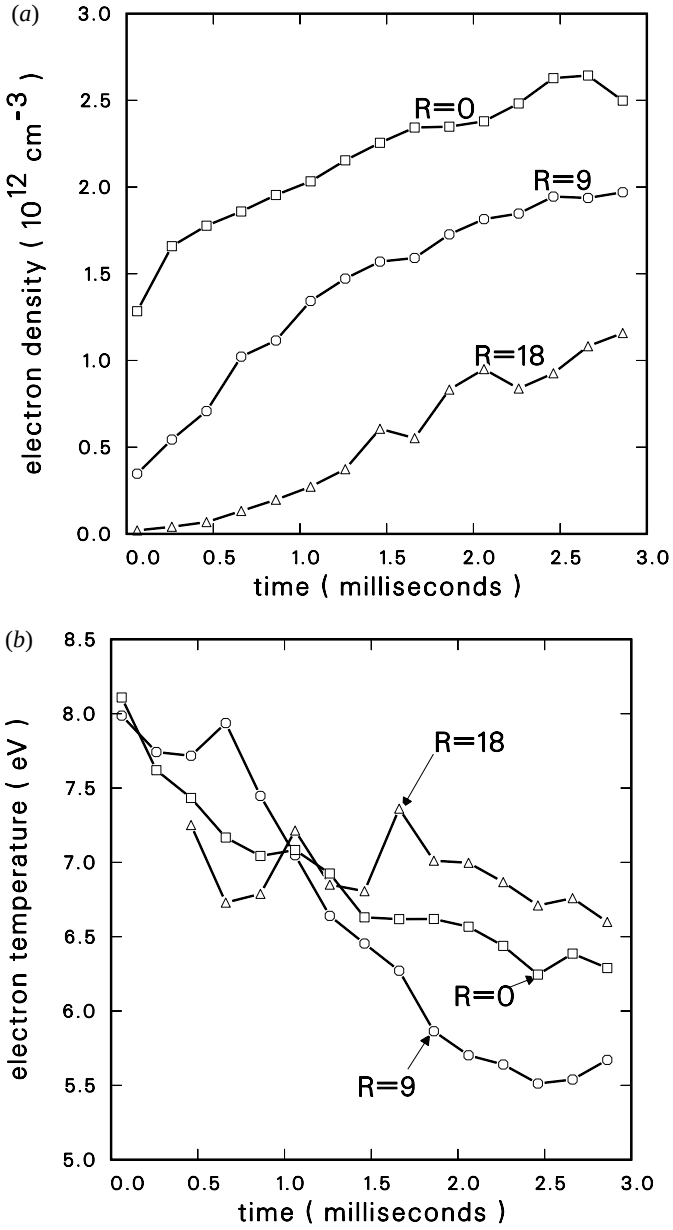

Figure 2. Measured values of electron density (*a*) and temperature (*b*) as a function of time at radial positions of $R = 0$, 9, and 18 cm from the centre of the LAPD plasma column.

The times shown in the figure are relative to an early threshold point (500 A) in the discharge current. The probe was located axially near the middle of the plasma column, at a distance of 5 m from the cathode. A time series of measurements was taken at three radial positions—$R = 0$, 9, and 18 cm from the centre of the column, the latter being near the plasma edge. The timing was controlled by an arbitrary function generator which produced a sequence of voltage ramps—a 100 μs-long ramp every 200 μs. The ramp signal was amplified to about 110 V

amplitude, biased to −90 V DC with respect to the grid anode, and applied to the Langmuir probe. Both the applied voltage and the resulting probe current were digitized and averaged over 30 shots.

The local electron temperature and density were computed by curvefitting the current trace for each voltage ramp, with calibration factors derived from microwave interferometry as discussed above. Each measured value characterizes a 20–30 μs interval in which the probe current makes its transition from ion to electron saturation. At $R = 18$ cm, our 1 mm^2 probe surface did not collect enough current to reliably extract the electron temperature for the first two time points. Otherwise, the average error for the electron temperature and density measurements was less than 5%.

3. Computational model

An atomic model for helium was calculated using the Los Alamos suite of atomic physics codes. The method for calculating the atomic structure is described elsewhere (Cowan 1981). The model includes each individual fine structure level designated by the usual $^{2S+1}L_J$ quantum numbers for all configurations of the type $1s^2$, $1s^1nl$, $2s^1nl$, and $2p^1nl$ in neutral helium and nl in ionized helium. All valid combinations of principle quantum number n and orbital angular momentum l through $n = 10$ and $l = 9$ were considered. Oscillator strengths for all dipole allowed transitions were also calculated. Therefore, all the singlet and triplet states in neutral helium through $n = 10$ are included individually and their associated optical transitions are resolved. In addition, a set of electron impact excitation, electron impact ionization and photo-ionization cross sections were calculated. First-order many-body (FOMBT) (Clark *et al* 1991a, Khakoo *et al* 1996) collision strengths were calculated for the $1s^2$–1snl, 1s2s–1snl and 1s2p–1snl transitions in neutral helium. For ionized helium, FOMBT was used for the 1s–nl, 2s–nl, and 2p–nl transitions. Plane wave Born cross sections (Cowan 1981) were used to fill in the remaining transitions. Therefore, both ground–excited and excited–excited transitions are considered. Electron impact ionization cross sections were calculated using the distorted wave method from the $1s^2$, 1s2s, and 1s2p levels of neutral helium. By comparison with distorted wave calculations, scaled hydrogenic cross sections (Clark *et al* 1991b) were found to be sufficently accurate for ionization out of other levels. Photo-ionization cross sections from all levels in each ion stage were calculated (Abdallah *et al* 1995) using the distorted continuum functions. Auto-ionization rates for the doubly excited states of neutral helium were also calculated for the inclusion of auto-ionization and dielectronic capture.

The level populations and free electron density are calculated by solving the rate equations as a function of time:

$$\frac{\mathrm{d}N_i}{\mathrm{d}t} = \sum_j A_{i,j}(N_e, kT_e)N_j, \tag{1}$$

$$\frac{\mathrm{d}N_e}{\mathrm{d}t} = \sum_{i,j} B_{i,j}(N_e, kT_e)N_j. \tag{2}$$

The N_i are the level populations, N_e is the electron density, kT_e is the electron temperature, the matrix A contains the rate coefficients of all processes initially in level j which populate level i and all processes which deplete the population of level i. The matrix B contains rate coefficients for all processes which produce or recombine free electrons. The rate coefficients for processes involving electron collisions are calculated by integrating the calculated cross sections over a Maxwellian energy distribution. Elements of the rate matrices A and B include multiplicative factors of N_e for processes induced by electron collisions. The equations are

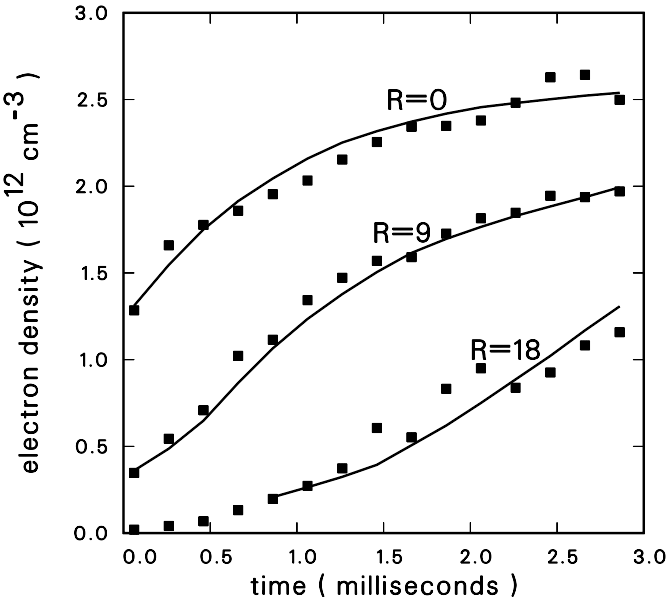

Figure 3. Comparison of the calculated electron density (full curve) with measured values (boxes) as a function of time for $R = 0$, 9, and 18 cm from the centre of the plasma column.

solved, given a set of initial conditions. The processes included are collisional excitation and de-excitation, spontaneous radiative decay, collisional ionization, three-body recombination, radiative recombination, auto-ionization and dielectronic capture. The plasma is assumed to be optically thin. Processes involving doubly excited states were found to be of little consequence for the plasma conditions under consideration and were subsequently discarded in the simulations to avoid unnecessary computation. Thus, equations (1) and (2) consisted of a set of approximately 300 coupled differential equations for this study. The details of the calculation are described elsewhere (Abdallah and Clark 1990).

4. Results

Figure 3 shows a comparison of experiment and calculation for the three radial positions in the plasma described previously. The starting point for the integration was the earliest measured time point for the $R = 0$ and $R = 9$ cases. The initial population density of He^+ was taken to be the measured electron density at that point, assuming that the He^{++} population density is negligible. The total density, neutrals plus ions, was fixed at the measured value of 2.6×10^{12} cm^{-3} for the integration. The measured temperatures at the succeeding time points which range from approximately 6–8 eV were then used in equations (1) and (2) to propagate the electron density to later times, which is shown by the full curves in the figure. The variation in electron density with radial position apparent in figure 3 is most likely caused by the discharge current spreading radially with time. Initially, the ionization rate is most rapid near $R = 0$ and slower at larger radial positions in the column.

The starting point for the $R = 18$ calculation was taken at a somewhat later time, 0.8 ms. In this case, the electron density is not well developed at early times, and the effects of the non-thermal discharge electrons are significant. An integration from an earlier time point yields a density curve that underestimates the ionization, consistent with the model used here which

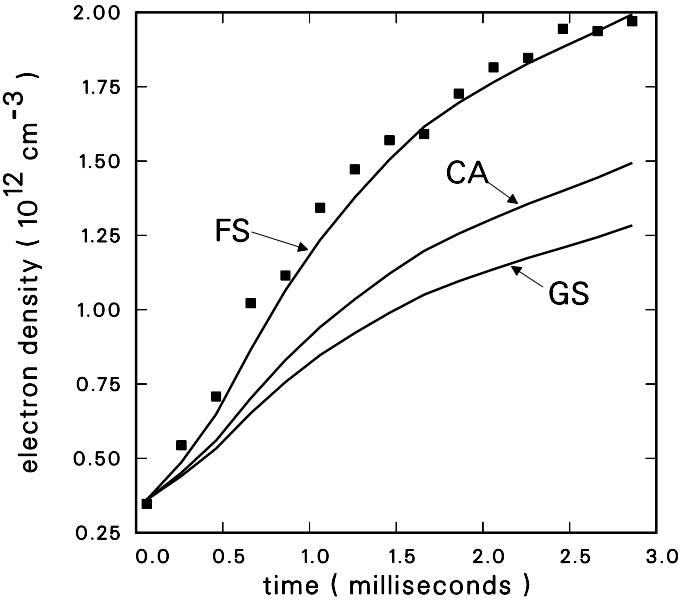

Figure 4. Comparison of the measured electron density at $R = 9$ cm as a function of time with calculations using different atomic models. FS is the fine structure model, CA is the configuration average model, and GS is the ground state model.

is based on Maxwellian electron energy distributions, and does not account for the action of the faster discharge electrons. Hence, the concept of electron temperature at early times and low electron density is ambiguous. However, once enough thermal electrons are produced, a reasonably good starting point is established, and the calculation is in agreement with the experiment.

The results discussed above were compared with the same calculations employing a configuration average model (Kilcrease *et al* 1993) which used the identical set of configurations and consistently calculated cross sections through $n = 10$, $l = 9$. A model including only the ground states in neutral He and He^+ was also constructed. The configuration average model includes excited states without metastables, and the ground state model includes no excited states with only direct collisional ionization allowed. The metastables are long-lived states in the fine structure model, whose radiative decay to the ground state is spin-forbidden. The three atomic models are compared to the $R = 9$ cm case in figure 4. The fine strucure calculation is in much better agreement with experiment than the simplified models which understimate the ionization.

Additional calculations for the $R = 9$ cm case were performed to test the sensitivity of the calculated electron density to the various processes included. The results show that a calculation including just collisional excitation, collisional de-exitation, radiative decay, and collisional ionization is nearly identical to the full calculation. Further, if collisional de-excitation is omitted, the result deviates by 4–5%. Thus, collisional excitation, radiative decay, and collisional ionization are absolutely neccesary while the effect of collsional deexciation is marginal. The influence of three body recombination, radiative recombination, auto-ionization, and dielectronic capture for a helium plasma under these conditions and in this time frame is negligible.

5. Conclusions

The local electron temperature and density have been measured at various times in a transient helium plasma at the UCLA LAPD. The rapid heating of electrons leaves the atoms in an underionized state compared to steady-state conditions for the typical electron temperatures that are observed. The measured temperatures were used in a time-evolving kinetics calculation to compare the predicted electron density with the measured values. The good agreement between calculated and measured density provides understanding of the experimental measurements, and confidence in the computational model.

The plasma is observed to be nearly fully ionized to He^+ in the centre of the column while it reaches only about 45% ionization at the edge. The model calculations are consistent with the measurements at three different radial positions using different initial conditions for the solution of the differential equations. The results show that bulk thermal secondary electrons control the plasma formation near the centre of the column about 0.8 ms earlier than at larger radial distances near the edge.

The importance of metastable excited states in a transient plasma is illustrated by comparing different atomic physics models with experiment. The results show a significant enhancement in ionization due to stepwise excitation–ionization of the metastable levels in neutral helium. Electron impact excitation builds up population in the long-lived metastable levels, which are then ionized directly by additional electron collisions. Inclusion of these levels proved to be essential to accurately predict the formation of the transient plasma encountered in the LAPD.

The model was also tested for sensitivity to the various atomic processes included. The results suggest that collisional excitation, radiative decay, and collisional ionization are predominant in the formation of the LAPD He discharge plasma, with collisional de-excitation making a small contribution. The influence of other processes such as three-body recombination, radiative recombination, auto-ionization, and dielectronic capture appears to be negligible.

Future work planned includes the study at early times in the discharge where non-thermal primary electrons are dominant, power balance calculations for predicting local plasma conditions, study of plasma properties after the discharge current has been switched off, and a spectroscopic analysis of the emitted radiation for diagnostic purposes, including laser-induced fluoresence.

Acknowledgments

This work was performed under the auspices of the US Department of Energy, the NSF under grant PHY-9309075, and the Office of Naval Research. JA acknowledges the Los Alamos Visiting Scholar programme for support of this work and thanks the UCLA Department of Physics for their hospitality. The authors also thank George Csanak for many useful discussions.

References

Abdallah J Jr and Clark R E H 1990 *Los Alamos National Laboratory Report* LA-11926 unpublished

Abdallah J Jr, Clark R E H, Kilcrease D P, Csanak G and Fontes C J 1996 *AIP Conf. Proc. 381: Atomic Processes in Plasmas (San Francisco, 1996)* ed A L Osterheld and W H Goldstein (New York: AIP) p 131

Abdallah J Jr, Collins L A, Csanak G, Petschek A G and Schappert G T 1995 *Z. Phys.* D **34** 233

Bamber J F, Maggs J E and Gekelman W 1995 *J. Geophys. Res.* **100** 23 795

Clark R E H, Abdallah J Jr and Mann J B 1991 *Astrophys. J.* **381** 597

Clark R E H, Csanak G and Abdallah J Jr 1991 *Phys. Rev.* A **44** 2874
Cowan R 1981 *The Theory of Atomic Structure and Spectra* (Berkeley, CA: University of California Press)
Fujimoto T 1979 *J. Quant. Spectrosc. Radiat. Transfer* **21** 439
Gekelman W, Pfister H, Lucky Z, Bamber J, Leneman D and Maggs J 1991 *Rev. Sci. Instrum.* **62** 2875
Gekelman W, Vincena S, Leneman D and Maggs J, 1997, *J. Geophys. Res.* **102** 7225
Goto M and Fujimoto T 1997 *National Institute for Fusion Science Research Report* NIFS-DATA-43 unpublished
Khakoo M A, Trajmar S, Wang S, Kanik I, Aguirre A, Fontes C, Clark R E H and Abdallah J Jr 1996 *J. Phys. B: At. Mol. Opt. Phys.* **29** 3477
Kilcrease D P, Abdallah J Jr, Keady J J and Clark R E H 1993 *J. Phys. B: At. Mol. Opt. Phys.* **26** L717
Pfister H, Gekelman W, Bamber J, Leneman D and Lucky Z 1991 *Rev. Sci. Instrum.* **62** 2884